Engineered Science

Embeddable Piezoelectric Sensors for Strength Gain Monitoring of Cementitious Materials: The Influence of Coating Materials

Yen-Fang Su,[1] Guangshuai Han,[1] Zhihao Kong,[1] Tommy Nantung[2] and Na Lu[1,3,4,*]

Abstract

It is critical to evaluate the quality of cementitious materials at its early age. Lead Zirconate Titanate (PZT) sensors, coupled with the electromechanical impedance (EMI) method, have proven to be a promising method for instantaneously monitoring the mechanical properties of cementitious materials. PZT is a piezoelectric ceramic with high piezoelectric properties and sensitivity, but its inherent brittleness limits its potential application in construction environments. To enhance the robustness of the sensor, this work has studied the use of two types of polymer coating as protective layers on the sensor, specifically Polydimethylsiloxane (PDMS) and polyester. The effectiveness of piezoelectricity in polymer-coated sensors is evaluated using a scanning laser Doppler vibrometer and an impedance analyzer. Finite element analysis has been conducted to simulate the frequency response of sensors with different coating configurations. Moreover, this study has evaluated the feasibility of monitoring the growth of mortars' mechanical properties over time using the proposed sensors with EMI technique. Based on the results, both polymer-coated sensors have shown adequate sensitivity in capturing the change of mechanical properties in cementitious materials. The polyester coating performed better durability than PDMS coating as encapsulating materials. It has been concluded that the polymer-coated, sensor-based EMI method can be an effective nondestructive evaluation method for monitoring concrete properties in practical applications.

1. Introduction

Cementitious materials gain strength rapidly during the hydration period, especially at its very early age (within the first 24 hours). At this stage, early-age cracks in the structure are susceptible to occur if the material quality is poor or the curing process is insufficient. The cracks might further propagate into unserviceable damage due to shrinkage and loading.[1] Thus, it is crucial to monitor the real-time mechanical properties of cementitious materials within the first 24 hours to ensure quality. The hydration process, where the cementitious materials strength gaining comes from, is relatively complicated and difficult to be evaluated in the field because it involves complex chemical compositions and reactions.[2-5] The maturity testing, which monitors the heat release during the hydration process, requires extensive calibrations of the maturity meter and trial batch for each different mix design, which is not very efficient. Therefore, it is essential to develop a reliable method that can efficiently monitor the strength gained during the material's very early age and predict its long term mechanical properties.[6]

Recently, piezoelectric materials, such as Lead Zirconate Titanate (PZT), have shown excellent performance for structural health monitoring (SHM).[7,8] Due to their unique direct and inverse piezoelectric effects, piezoelectric materials can convert mechanical property into electrical signals and vice versa. As such, these materials are suitable to be fabricated into actuator and transducer for sensing applications.[9,10] Among all the piezoelectric materials, PZT has superior piezoelectric properties and high sensitivity; it can capture the mechanical impedance of a structure through the electromechanical impedance (EMI) technique. Researchers have also

[1]*Lyles School of Civil Engineering, Sustainable Materials and Renewable Technology (SMART) Lab, Purdue University, 550 Stadium Mall Drive, West Lafayette, IN 47907-2051, USA.*

[2]*Office of Research and Development, Indiana Department of Transportation*
[3]*School of Materials Engineering, Purdue University.*
[4]*Center for Intelligent Infrastructure, Purdue University.*
 * *E-mail: luna@purdue.edu (N. Lu).*

used the PZT sensor to monitor the hydration process of cementitious material.[11-16] The results indicated that the EMI signal responses could reflect the different hydration stages over time. The piezoelectric sensors are typically placed in two configurations: mounted on the surface or embedded into its host structure. Surface mounting is a conventional method of bonding the PZT patch to the host structure by using high-strength adhesive. In this case, the bonding layer is assumed to be a thin bar in order to transform vibration caused by alternative voltage.[17] Guo et al. soldered the coppery paper and the PZT patch to the top surface of the concrete to perform the EMI experiments.[18] The results showed that the EMI spectrums could serve as indicators for the concrete hardening process over time. Lee et al.[19] used conductive adhesive to bond the PZT patch to the sides of the concrete. They observed the shifting in EMI spectrums due to moisture loss and strength gain as the concrete aged. Su et al. used the surface bonding method to precisely correlate the cementitious materials' very-early-aged compressive strength with statistics indices and the indices of phase angle from EMI signals.[13,16,20] It has been concluded that all of these surface bonding methods require choosing the particular adhesive with a suitable bonding strength and mechanical interaction between the sensor and the host structure.[21] Several attempts have also been made to fabricate reusable PZT transducers by means of indirectly bonding PZT with substrates. Yang et al.[22] developed a concrete hydration setup using an aluminum enclosure. The PZT was first bonded with the aluminum enclosure then inserted into the concrete. The proposed setup displayed a comparable sensing efficiency with the surface bonded PZT. Lu et al.[22] designed a smart probe by prefabricating a PZT transducer with an aluminum flat bar. The results showed that the compressive strength and the elastic modulus could be assessed based on information from the EMI spectrum. The need to protect brittle PZT and early age installation, however, has not been fully addressed.

Although the PZT patch has exhibited its potential to capture the cementitious materials' hydration and strength gain process as a sensor, the PZT's intrinsic brittleness and vulnerability limit the application in realistic environments.[9] It has been observed that there are thin, brownish cuprous oxides on the copper-nickel (CuNi) contact of the nude PZT patch, which would affect the measurement results.[23] Besides, the sensor can only be surface bonded on the concrete sample after the initial setting, which limits the possibility of using sensors to obtain the information on the concrete before its initial setting. The properties of concrete might exhibit some differences between its surface and interior, especially for the thicker concrete pavement. Thus, the protective layer is needed to enable the PZT sensor to be embedded in the concrete structure. Mostly, the embeddable PZT sensor is fabricated by assembling interconnectors, mounting adhesive, and bonding layers to avoid the harsh construction environment. The wrapping methods include the use of rubber as a protective layer in order to fabricate a sandwich-like piezoelectric sensor,[24] a semi-spherical styrene embedded piezoelectric sensor,[25] an epoxy wrapped sensor,[26] and asphalt binder coated PZT sensors.[27]

In addition to the aforementioned wrapping method, a couple of stiff coating methods have also been investigated.[12,28,29] For instance, Li et al. developed a cement-based piezoelectric sensor to evaluate the responses of different loading conditions, and Kong et al. slipped a PZT patch between two marble blocks to manufacture smart aggregates (SA) to be a substitute for a coarse aggregate while acting as a sensor.[12] Saravanan et al.[28] used butter paper as a mold with a layer of ordinary Portland cement paste or adhesive on the soft PZT sensor to fabricate the smart clinker. It has concluded that the flexible adhesive-coated sensor revealed more information in the material's early ages, yet the hardened cement paste-coated sensor is more suitable for long-term monitoring.

Table 1 summarizes different methods of fabricating embeddable PZT sensors. Although these sensors can serve specific purposes in their studies, the effectiveness of piezoelectricity and the durability of these sensors were not evaluated. The coating or protecting layer might affect the sensing outcome due to attenuation. Soft coatings, such as asphalt, epoxy, and rubber, might absorb the vibration and weaken sensing ability accordingly. As for stiff protecting layers like cement paste, they are unstable due to the continuous hydration process. The cement pastes typically need more than 90 days to become fully hydrated; further, the water in the fresh concrete might react with a cement paste-capsuled sensor. Besides, the steel washer and marble block are not cost-effective for broad application.

Unlike the previous work, this study has investigated two types of polymer coatings meant to encapsulate the PZT sensor in order to improve durability and the ability of implementation. The two types of polymers used as coating materials are flexible Polydimethylsiloxane (PDMS) and rigid polyester. The sensor properties of the proposed thin coating layer were investigated with a scanning laser Doppler vibrometer (LDV) and an impedance analyzer. The finite element simulation was also conducted using ABAQUS FEA to analyze the sensors with different coating configurations. The polymer-coated sensors were further used for monitoring strength gain and stiffness growth for cementitious materials from a very early age (6th hour to 12th hour) to an early age (1st, 3rd, and 7th day). The EMI measurement and the compressive test (ASTM C109) are conducted simultaneously to evaluate the correlation between sensing results and mechanical properties. Finally, the effectiveness of the polymer coating is discussed in order to come up with a better polymer-coated sensor for monitoring the growth of the internal mechanical properties of cementitious materials with high accuracy.

Table 1. Literature for different methods aimed at protecting PZT sensors.

Reference	Application	Coating/Protecting layer	Indicators
2006 Chen *et al.*[24]	Stress indicator	Silicon rubber	Piezoelectric dissipation factor
2006 Li *et al.* [30]	Monitoring traffic flow	Cement paste	Output of sensors
2006 Annamdas *et al.*[31]	Health monitoring	Steel washer	Admittance signatures
2009 Li *et al.* [32]	Concrete Diagnosis	Epoxy	Longitudinal and transverse velocities
2010 Annamdas *et al.* [26]	Damage analysis	Epoxy & Cement	Statistical indicators
2014 Kim *et al.*[25]	Strength estimation	Styrene	Resonant frequency
2014 Wang *et al.*[11]	Early age strength	Asphalt	Statistical indicators
2014 Kong *et al.*[12]	Hydration monitoring	Marble block	Amplitude level and frequency domain
2015 Wang *et al.*[27]	Health monitoring	Asphalt	Statistical indicators
2016 Ai *et al.*[7]	Damage detection	Cement encapsulation	Statistical indicators
2017 Narayanan *et al.*[15]	Hydration monitoring	Hydrophobic coating& Epoxy layer	Effective mechanical impedance
2017 Saravanan *et al.* [28]	Damage detection	Cement paste & Adhesive	Statistical indicators

2. Experimental program

2.1 Fabrication of polymer-coated sensor

In this study, two types of polymer were used as the coating materials for the sensors: polyester resin and Polydimethylsiloxane (PDMS). Polyester is a thermoset resin with a high elastic modulus of around 33 GPa. Its great chemical resistance and mechanical properties make it preferable to be applied in the marine industry. Also, it exhibits relatively low shrinkage (4%-8%) during curing.[33] Unsaturated polyester (UPR) was mixed with a 1.5% volume ratio of styrene (ethenylbenzene) monomer for 15 minutes. The prepared PZT sensors were dipped into the liquid polyester resin twice to ensure the coating's performance. The coated sensors were cured at 23±2 °C for 18 hours and later placed in a 60 °C chamber for another 6 hours. In comparison, PDMS (CH$_3$[Si(CH$_3$)$_2$O]$_n$Si(CH$_3$)$_3$), a flexible thermosetting polymer, was also employed as a sensor coating. The elastic modulus of PDMS ranges from 1.3 to 3 MPa. It also has good chemical resistance and is hydrophobic. The shrinkage of PDMS is around 0.3% -1.8%, depending on curing temperature.[34] Two-parts silicone encapsulant (pre-polymer base and a cross-linking curing agent) was mixed for polymerization and cross-linking. The sensors were coated with PDMS twice and cured at 23±2 for 24 hours. The schematic of the sensor's structure is shown in Fig. S1.

2.2 Characterization of sensor

2.2.1 LDV measurement

The laser Doppler vibrometer (LDV) system was employed to measure the amplitude of vibration (displacement) of the piezoelectric sensors under different electric potentials. As Fig. S2 (a) shows, the LDV system (Polytech MSA 400) consists of an LDV sensor head with laser, junction box, controller, data acquisition, and Polytech laser vibrometer (PLV) software. The schematic detailing LDV measurement is shown in Fig. S2 (b). Based on the Doppler effect, the vibrometer uses a two-beam laser to measure the interference between the test beam and the internal reference beam. The piezoelectric sensor was set on the optical table below the objective microscope lens and connected to the system to receive the exciting voltage for vibration. A helium-neon laser was focused on the sample to retrieve the scattered laser light back. The measurement of velocity or displacement can be obtained through monitoring a grid of points where the laser spot pointed on the sample. The resolution of this LDV system is 2 nm for deflection measurement.

2.2.2 EMI analysis

The EMI measuring system, as Fig. S3 (a) shows, consists of an impedance analyzer and a laptop equipped with data collection/analysis software. The piezoelectric material-based EMI technique is based on the piezoelectric effect (direct and inverse effect). The impedance analyzer generates an alternating current to excite the piezoelectric sensor at a frequency range from 5 kHz to 1000 kHz, with the sampling rate of 10 MHz. Then, the sensor receives the electromechanical dynamic response through the sensor, as Fig. S3 (b) presents. Based on Ohm's law, the impedance (Z) can be obtained by calculating the sinusoidal voltage (V_{AC}) and alternative current (I) from the EMI measurement as equation (1) expresses:

$$Z = Z_R + Z_L = V_{AC}/I \qquad (1)$$

where, for inductor: $Z_L = j\omega L$, j is $\sqrt{-1}$, ω is the angular frequency, and L is inductance.; for a resistor: $Z_R = R$ and R is resistance.

For AC circuit analysis, V_{AC} and I can be expressed as a complex number through Euler's formula as equation (2) below:

$$I = \frac{V_0 e^{j(wt-\theta)}}{\left[R^2+(\omega L)^2\right]^{1/2}} \qquad (2)$$

where V_0 is the amplitude of the sinusoidal voltage, θ is the phase angle, and t is the time.

2.3 Monitoring the mechanical properties of cementitious material

One of the primary objectives of this study is to verify the feasibility of polymer-coated sensors for monitoring the mechanical properties of cementitious material. The EMI technique was conducted simultaneously with the mechanical test at each age of interest. The EMI signals obtained from the sensor were post-processed using the commonly-employed statistical method of the root-mean-square deviation index (RMSD) [13,14,35-43] to quantify the change of spectrum with time. Finally, the linear least squares regression analysis was conducted to evaluate the correlation performance of the sensor with different configurations.

2.3.1 Preparation of cementitious material

As Table 2 shows, type I Ordinary Portland Cement (OPC), class C fly ash, and silica sand were used for casting the 2" cubic specimen with a water-to-binder ratio of 0.42. The samples were prepared for testing at a very early age, from 6 to 12 hours, with the 2-hour increments after casting and during their early age (1st, 3rd, and 7th days).

Table 2. Mixture design (lbs/yd^3).

Cement	Fly Ash-C	Sand	Water	Water Reducing Agent
524.3	78.6	1572.8	219.3	1048.5 ml/yd^3

2.3.2 EMI for monitoring the properties of cementitious material

The PZT sensors were embedded within or surface mounted on the mortar cube to measure the dynamic impedance (Z) of the PZT sensor and host structure. An electric potential of 0.5V was applied to the PZT sensor through the impedance analyzer. The dynamic electromechanical response of the PZT-structure interaction can be described using the theoretical admittance equation, as seen in Equation (3).[20]

$$Y = G + Bj = 4\omega \frac{l^2}{h}\left[\overline{\varepsilon_{33}^T} - \frac{2d_{31}^2\overline{Y^E}}{(1-v)} + \frac{2d_{31}^2\overline{Y^E}}{(1-v)}\left(\frac{Z_a}{Z_a+Z_s}\right)\frac{tan\,kl}{kl}\right] \quad (3)$$

The measured electrical impedance (reciprocal of admittance) of the PZT sensor is mainly induced by the mechanical impedance of the free PZT sensor (Z_a) and that of the host structure (Z_s). The admittance is a function of the real part-conductance (G), and the imaginary part- susceptance (B) with its imaginary unit (j). Other than the mechanical impedance, the material properties are incorporated in the function, with the dimensions of the PZT sensor (w, l, and h - width, length, and height), piezoelectric coefficient (d_{31}), electrical permittivity $\overline{\varepsilon_{33}^T}$, ($\overline{\varepsilon_{33}^T}=\varepsilon_{33}^T(1-\delta j)$), Poisson's ratio ($v$), wavenumber ($\kappa$), and dynamic Young's modulus ($\overline{Y^E}$, ($\overline{Y^E}=Y^E(1+\eta j)$)).

2.3.3 Compressive test

Conventional cube compressive tests per ASTM C109 and EMI testing were conducted simultaneously to assess the potential of polymer-coated PZT sensors in monitoring the strength of cementitious materials. The applied compressive loading was controlled within a range of 900 N/s to 1800 N/s on the 50 mm cubic specimens. The tests were executed at a very early age (6th hour to 12th hour) and during early age (1st, 3rd, and 7th days). Three compressive specimens were tested and averaged at each age of interest.

3. Simulation of polymer-coated PZT sensor

The finite element model of the PZT sensor was built using ABAQUS/Standard (Dassault Systèmes Simulia Corp., US) to investigate the effect of coating materials on EMI signals. Two types of polymer, i.e., polyester and PMDS, were investigated through simulation. The density of polyester is 1.09×10^{-9} ton/mm^3, its elastic modulus is 3300 MPa, its Poisson ratio is 0.33, and the structural damping is 0.5. The density of PDMS is 1.06×10^{-9} ton/mm^3, its elastic modulus is 3 MPa, its Poisson ratio is 0.48, and the structural damping is 0.2. The material properties of PZT are shown in Table 3. It should be noted that, in the piezoelectric area, the direction convention is as such: 1, 2, 3, 4, 5, 6 correspond to X, Y, Z, YZ, XZ, XY, respectively. The polarization direction of the PZT patch is along with the three directions (the normal direction of the PZT patch). The piezoelectric equation is of strain type, and the unit of the piezoelectric constant is C/N or m/V. The structural damping of PZT is set as 0.1.

The objective of FEA is to discuss the effects of polymer coating and coating thickness on EMI testing. The thickness of the PZT patch is 0.2 mm in all sensor models. The total thickness of the sensor is set to be 0.5 mm (with 0.15 mm coating), 1.0 mm (with 0.40 mm coating) and 1.5 mm (with 0.65 mm coating), as shown in Fig. S4 (b), (c), and (d), respectively. The element size along the thickness direction is 0.05 mm and the element size orthogonal to the thickness direction is 0.5 mm for all models. An example is shown in Fig. S5. The PZT sensor is in the free boundary condition. The contact between PZT and coating is accomplished by hollowing out the coating material, then bonding the PZT and hollowed coating using a "tie" constraint.

Table 3. Material properties of PZT.

Density (ton/mm³)	7.80×10^{-9}		
Dielectric constant (10⁻¹⁴ farad/mm)	D11	D22	D33
	1.0	1.0	0.5
Elastic modulus (MPa)	$\begin{bmatrix} 120000 & 77800 & 74300 & 0 & 0 & 0 \\ 0 & 120000 & 74300 & 0 & 0 & 0 \\ 0 & 0 & 110000 & 0 & 0 & 0 \\ 0 & 0 & 0 & 25600 & 0 & 0 \\ 0 & 0 & 0 & 0 & 25600 & 0 \\ 0 & 0 & 0 & 0 & 0 & 30580 \end{bmatrix}$		
Piezoelectric constant (10⁻¹⁰ C/N)	$\begin{bmatrix} 0 & 0 & 0 & 0 & 5.5 & 0 \\ 0 & 0 & 0 & 5.5 & 0 & 0 \\ -2.1 & -2.1 & 5.0 & 0 & 0 & 0 \end{bmatrix}$		

The electrical potential on one side of the PZT patch is set to 0 and, on the other side, it is set to be a sinusoidal wave with an amplitude of 1.0 V (while the value input into ABAQUS is 1000 because of the s-mm-ton-A unit system) using a steady-state dynamic analysis. The output variable of interest is the electrical admittance Y of the PZT sensor, and Y is determined with $Y=i\omega\sum Q$, where ω is the angular frequency and $\sum Q$ is the summation of nodal charge on one side of the surface of PZT.

The analysis is performed by the "Steady-State Dynamics, Direct" procedure of ABAQUS. The procedure can be used for coupled acoustic-structural medium, piezoelectric medium analysis, and viscoelastic material modeling. The formulation is based on the dynamic virtual work equation:[44]

$$\int_V \rho \delta u \cdot \ddot{u} dV + \int_V \rho \alpha_c \delta u \cdot \dot{u} dV + \int_V \delta \varepsilon : \sigma dV - \int_S \delta u \cdot t dS = 0 \quad (4)$$

where the ρ denotes the density, u denotes the displacement field, α_c denotes the mass proportional damping factor (part of the Rayleigh damping assumption), $\delta\varepsilon:\sigma$ denotes the rate of internal work per volume, V denotes the volume, S denotes the surface, and t denotes the surface traction.

4. Result and Discussion
4.1 Behavior of Free PZT sensors

The displacement results of three configurations of PZT sensors measured via LDV are exhibited in Fig. 1, including uncoated, PDMS-coated, and polyester-coated PZT sensors. The applied voltage changed from 0.1V to 4V to measure the displacement of the sensors. It is not surprising that the uncoated PZT sensor has the highest slope of the curves from 0.1V to 1V, in which the slope represents the piezoelectric constant d_{33}. The PDMS-coated sensor shows a similar yet lower slope than the uncoated sensor due to the polymer coating restraining the vibration of piezoelectric materials. Furthermore, owing to the high stiffness of polyester, the coated sensor exhibited the lowest slope.
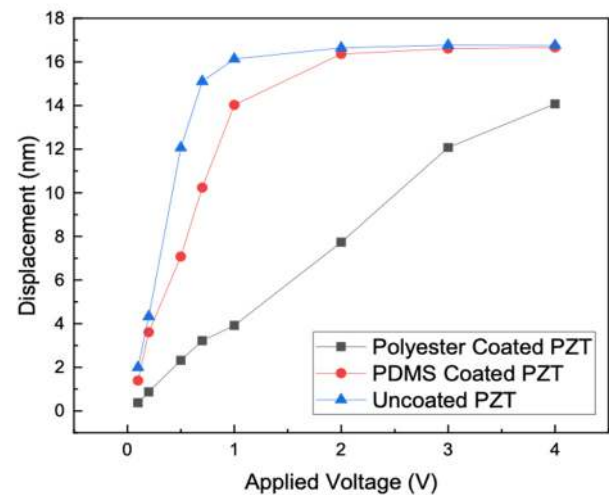

Fig. 1 The LDV displacement results of three type of sensor under different applied voltages.

Fig. 2 (a) and (b) compare the conductance spectrum of two types of polymer-coated PZT sensors. It can be observed that there are four major humps in the conductance spectrum of the uncoated PZT sensor due to the resonance at the frequency ranges of 0 to 200kHz, 300kHz to 500kHz, 500kHz to 800kHz, and 800kHz to 1000kHz, respectively. At the ranges of 0 to 200kHz and 300kHz to 500kHz, the uncoated and polyester-coated sensors performed multi-split peaks; the PDMS-coated sensor, however, performed two-step peaks. Starting from 500kHz, the polyester sensor did not show a significant hump; in other words, the anti-resonance is ambiguous. At the high-frequency range from 800kHz to 1000kHz, the PDMS-coated sensor turns to the single domelike eminence.

These observations of the polymer-coated sensors are owing to the characteristics of a different polymer. After condensation polymerization, the unsaturated polyester reacted with styrene at the elimination of water to form high stiffness polyester. Thus, the polyester-coated sensor confined the degree of freedom of PZT, resulting in the lower conductance and multi-split peaks. Similarly, the susceptance and admittance spectrum of the polyester-coated sensor, shown in Fig. 2 (c) and (e), indicated that the coating suppressed the amplitude of signals.

On the other hand, elastomeric PDMS might absorb the vibrations; thus, the conductance spectrum of the PDMS-coated sensor (Fig. 2 (b)) exhibits smoother (less sharp peaks). Also, the PDMS did not strictly restrict the vibration of the PZT sensor. Hence, the conductance of the coated sensor and the uncoated sensor has a similar amplitude. The suppression is also exhibited in the admittance spectrum of the PDMS coated sensors, as Fig. 2 (f) shows. In Fig. 2 (d), the susceptance of PDMS at most frequency bands do not show significant difference except at the frequency around 200 kHz. The interesting oscillation on the susceptance spectrum of both uncoated and PDMS-coated sensors should be further discussed in future work.
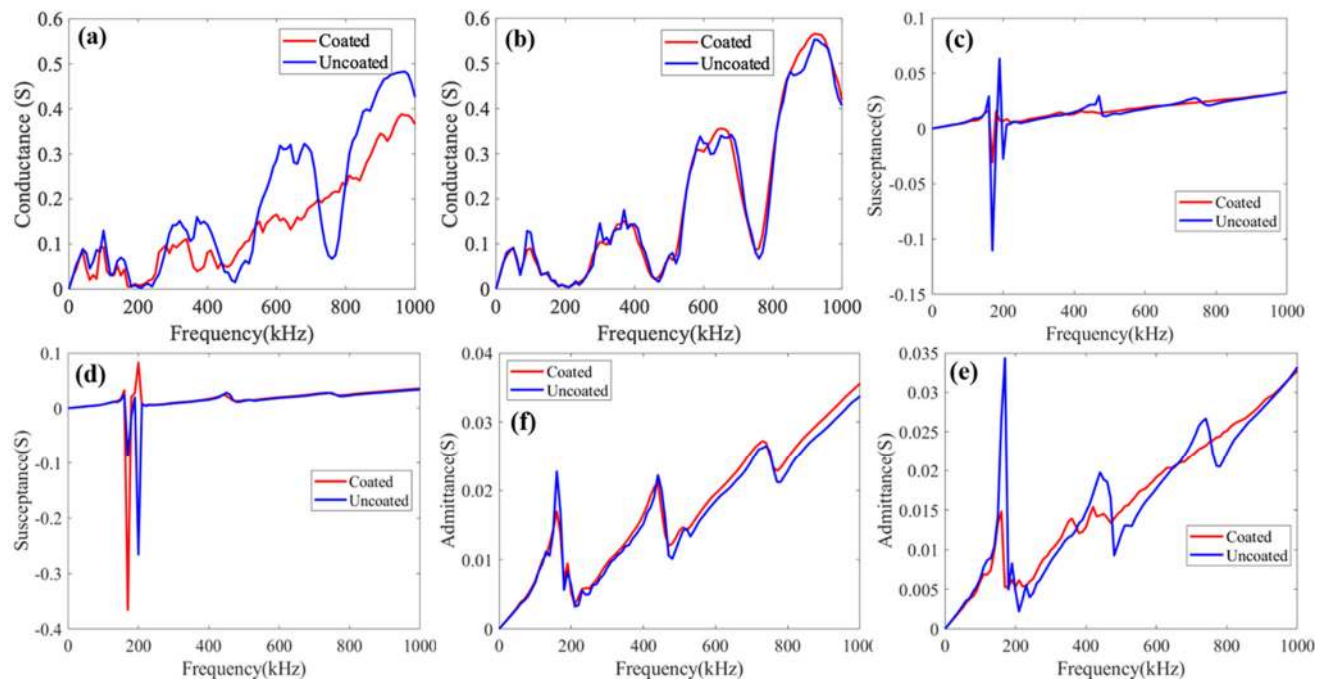
Fig. 2 Spectrums of two types of polymer-coated sensors and uncoated sensors: (a) Conductance of polyester-coated sensor; (b) Conductance of PDMS-coated sensor; (c) Susceptance of polyester-coated sensor; (d) Susceptance of PDMS-coated sensor; (e) Admittance of polyester-coated sensor; (f) Admittance of PDMS-coated sensor.

4.2 Simulation results of the polymer-coated sensors

The FEA was conducted to ascertain assumptions from the experimental observations. Fig. 3 compares the experimental results with the simulation results for the uncoated PZT sensor. It can be seen that the first resonance peak of the simulated admittance spectrum is perfectly in line with the experimental result. The amplitudes of other peaks are not totally matched together due to the uncertainty of dielectric loss and mechanical loss; the location of each simulation resonance peak, however, is aligned with the experiment. This model was further used to analyze the influence of the coating materials and the coating thickness.

The finite element simulation results are present in Fig. 4 (a) for uncoated sensors, and Fig. S6 (a)-(f) for different polymer-coated sensors. The tomographic colors reveal the distribution of electric charge results (RCHG) in coulomb (C) at the frequency frame of the first resonant peak (around 160 kHz). As can be observed in Fig. 4 (a), the electric charge of the uncoated PZT sensor is mainly dispersed around in the middle as the circle on the x-y plane.

Fig. S6 (a), (c), and (e) show the polyester-coated sensor with different coating thicknesses, including 0.5 mm, 1.0 mm, and 1.5 mm, respectively. It can be seen that the diameter of the red circle decreases with increases in coating thickness since the inherent rigidity of polymer constrains the degree of freedom for vibrating. In Fig. S6 (b), (d), and (f), however, with the increase of thickness for the PDMS coating, the sensor did not show much difference in performance. For the same polymer coating thickness, PDMS presents less of a constraining effect than polyester coating because of its inherent elastomeric property. To be more specific, the flexible

PDMS provides less restriction to the sensor. To quantify the constraint effect, Table 4 provides the integrated electric charges of different configurations of sensors and the ratio with the uncoated sensor (RU). It is apparent from this table that the polymer coatings lead to the decrease of electric charge in the sensor. The integrated electric charges decrease as the coating increases in thickness. The RU of 0.5 mm polyester coating is 0.63 and significantly reduces to 0.14 for a thickness of 1.0 mm. The PDMS-coated sensor with three different thicknesses, however, shows similar RU results around 0.88-0.89. A possible explanation for this might be that the stiffness of coating material affects the constraining force. Another possible reason might attribute to the adhesion, which needs to be further investigated.
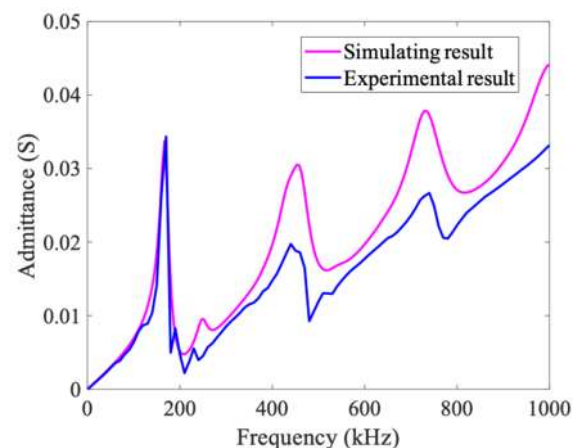
Fig. 3 Comparing the simulation result with the experimental result of uncoated PZT sensor.
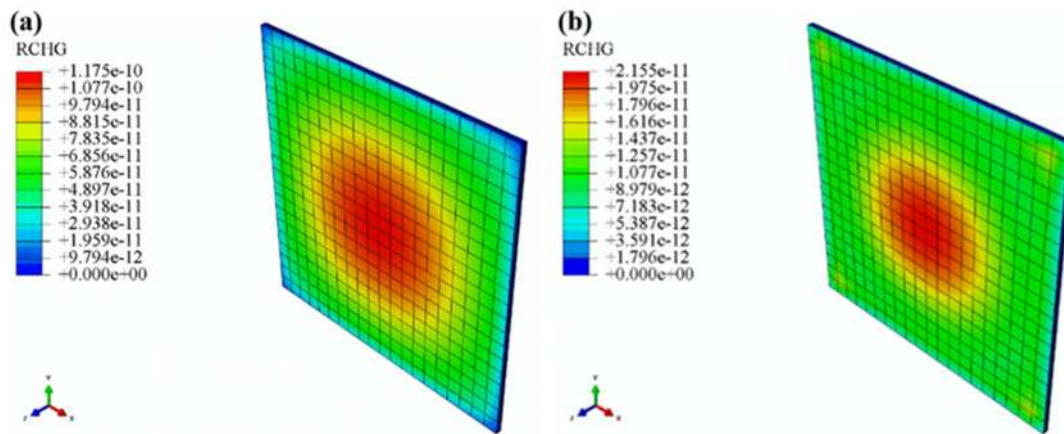
Fig. 4 FEM electric charge results of different configurations of PZT sensors, (a) Uncoated PZT sensor; (b) 1.0 mm polyester coated.

Table 4. Electric charge of sensors.

Configuration	Integrated electric charge of sensor (C)	Ratio with uncoated
Uncoated	2.93815E-008	1
0.5 mm polyester coated	1.84396E-008	0.63
1.0 mm polyester coated	5.15300E-009	0.18
1.5 mm polyester coated	4.21349E-009	0.14
0.5 mm PDMS coated	2.59839E-008	0.88
1.0 mm PDMS coated	2.61823E-008	0.89
1.5 mm PDMS coated	2.61986E-008	0.89

Fig. 5 (a) and (b) display the simulation results of two types of polymer-coated PZT sensors with different coating thicknesses from 0.5 mm to 1.5 mm. It can be observed that the thickness of polyester coating has a more significant influence on the admittance spectrum than PDMS coating due to its inherent higher stiffness. The thicker the polyester coating, the lower the amplitude of the sensor's admittance. Also, the spectrum tends to shift leftward with the thickness increase. On the other hand, the PDMS coating only slightly drops the admittance with increasing thickness. To sum up, the simulation results agree with the experimental observation and our explanation.

4.3 PZT sensors for mortar properties monitoring

Previous studies have revealed that the surface-bonded piezoelectric sensor can instantaneously monitor the strength development of cementitious materials at an early age via the EMI method.[13,14,16] However, the rough surface condition of the host structure would affect the bonding interface, which might influence the quality of measurement. Moreover, the sensor cannot be surface mounted on the cementitious materials with delayed setting time to monitor the properties at its very early age. The polymer-coated sensor can directly bury in the cementitious materials during casting, which enables the sensor to capture the property changes of materials from the beginning.

Fig. S7 (a) to (f) demonstrate the EMI signal of mortar samples obtained from three types of sensors from a very early age (6 hours to 12 hours) and to an early age (1 to 7 days) of the cementitious sample. It can be observed that the PZT sensors captured the conductance and susceptance spectrum changes with time. During this hydration period, nucleation and growth begin to accelerate dramatically. Hydration of C_3A (alite, the main phase of OPC) accelerates to form C-S-H (calcium silicate hydrate) and $Ca(OH)_2$ (portlandite).[2] The hydration products lead to a solidification of mortar and a decrease of porosity, resulting in the stiffness growth of cementitious materials. The spectrum shifting rightward with time is attributed to the state of mortar consistency changing from plastic to rigid. After one day, the skeleton of microstructure forms in the mortar sample; thus, it exhibits more multi-split peaks on the spectrum.

Fig. S7 shows the spectrum results of polyester-coasted sensors. As mentioned, the rigid property of polyester dropped the conductance of the sensor. Thus, there is no eminence in the spectrum after 200 kHz at the mortar's very early age. The two-peak hump, however, appeared on the conductance signals collected after one day. The interesting observations might be attributed to the solidification and water evaporation of cementitious materials over time. To be more specific, the shifting trend of the spectrum is due to the hydration of cementitious materials, which led to the gradational growth of stiffness. If we inspect the smoothness of the spectrum, it can be found that the signal obtained from PDMS sensors —Fig. S7 (c) and (d)— is smoother than the others due to the energy absorption of elastomeric PDMS coating. The smoother signals are more distinctive for observing the progressive trend in cementitious materials during hydration.
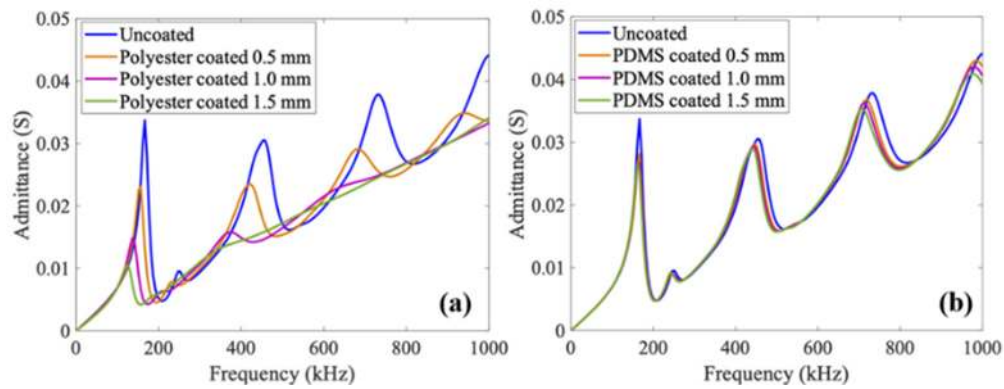
Fig. 5 Simulation results of polymer-coated PZT sensors with different coating thickness: (a) Polyester; (b) PDMS.

To validate the feasibility of the polymer-coated sensor, a linear least-squares regression analysis was employed to assess the correlation between the statistical RMSD index and the compressive strength results using polymer-coated sensors. The EMI results of the uncoated sensor were also displayed for reference. Fig. 6(a) and (b) present the regression results between mechanical properties and the EMI-RMSD index of three configurations of the sensor. It can be seen that the regression results (R^2) for all sensors are above 0.95, which indicates the EMI-RMSD obtained from all types of sensor perform accurately at monitoring the compressive strength gain. The elastic modulus results in Fig. 6(b) also present a high correlation of R^2 greater than 0.9, with the EMI-RMSD index calculated from the sensors. The slope of each data set in Fig. 6(a) and (b) represents the sensitivity of the sensor on monitoring mechanical properties. The results indicate that the uncoated PZT sensor has a higher sensitivity than coated sensors. Nevertheless, the thin polymer coatings with relatively lower sensitivities did not affect the performances of the sensors at capturing the property changes of cementitious materials.

Compared with other NDT methods, the sensing performance of the proposed EMI method is equal to or even better than other concrete NDT methods, including the maturity method, and ultrasonic pulse velocity (UPV). The accuracy of the maturity method[45] typically ranges from 0.85 to 0.9, and the regression analysis results of UPV[46] are generally below 0.9 for estimating the early age mechanical properties of cementitious materials. The outcome here ascertains that the polymer-coated sensor embedded in cementitious materials can effectively monitor changes to mechanical properties with high accuracy.

4.4 Interfacial properties of polymer coating

Besides the sensing performance, the durability and robustness of sensors are essential for practical application, especially in harsh concrete construction. Although the PDMS-coated sensor exhibited an excellent sensing performance, the peeling off some of the PDMS coatings has been observed due to copper-nickel (CuNi) contact on the PZT surface. On the other hand, the polyester coating presents better robustness than PDMS. It is known that the adhesion of the polymer has a close relationship with surface energy.[47] Based on the Young-Dupré equation,[48] the relationship between adhesion and surface energy can be described as below:

$$W_{12}=\gamma_1+\gamma_2-\gamma_{12}$$

where W_{12} is the energy of adhesive, γ_1 and γ_2 represent the surface energies of two materials, and γ_{12} is the interfacial energy between surfaces 1 and 2. The higher the surface energy, the stronger the adhesion. The surface energy of polyester 20 °C is around 40-50 mN/m;[49,50] it is only 15-20 mN/m[49,51] for PDMS. Thus, PDMS is more vulnerable to peeling off from the substrate.
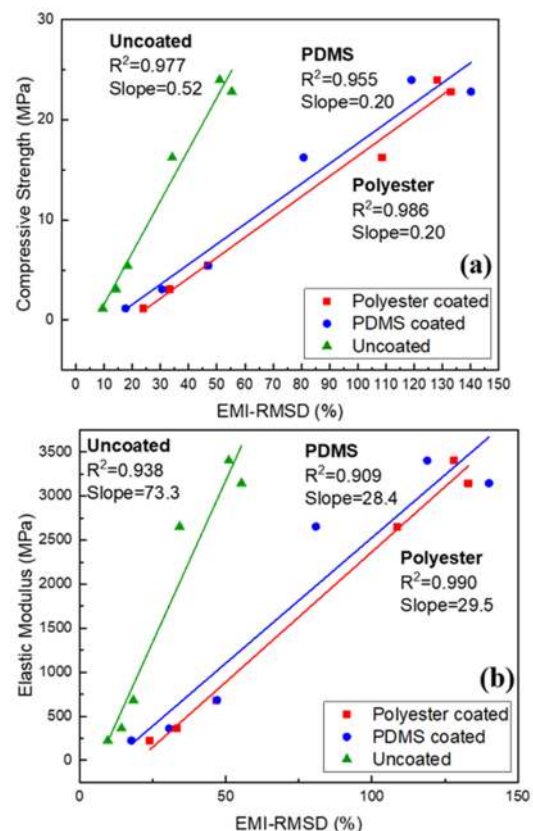

Fig. 6 Mechanical properties vs. EMI-RMSD index of three configurations of the sensor for mortar strength monitoring: (a) compressive strength vs. EMI index, (b) elastic modulus.

5. Conclusion

In this study, two kinds of polymers have been investigated as coatings on PZT sensors, including a rigid polymer (polyester) and a soft polymer (PDMS). The performances of sensors were characterized using a scanning laser Doppler vibrometer and an electromechanical impedance analyzer. FEA was used to study the frequency response of the PZT sensor with different polymer coatings. The coated PZT sensors were further used for monitoring the mechanical properties of cementitious materials. The EMI technique was applied with statistical data processing methods to validate the feasibility of polymer-coated sensors compared with the uncoated sensors used in previous studies. The summary of this study is presented as follows:

1. For the sensor characterization, the LDV results indicate that the voltage-displacement curve of the polymer-coated sensors showed a lower slope at the voltage range from 0.1V to 1V. It might be due to the polymer coating restraining the vibration of piezoelectric materials. The polyester coating has a higher stiffness, which resulted in the lowest slope. The electrical response of polymer-coated sensors was investigated through an impedance analyzer. The polymer coating affected the signals of the spectrum. The elastomeric property of PDMS might absorb some vibration, resulting in the smoothing of the spectrum. Nonetheless, the stiffer polyester coating exhibits more multi-split peaks in the conductance spectrum, which is attributed to the polyester confined to the PZT's degree of freedom. The admittance and susceptance spectrums agreed with the phenomenon, as mentioned above.

2. The finite element analysis was applied to simulate the influence of polymer coating and discuss the thickness effect of the sensor. The results suggest that stiffer polyester coating showed a more significant influence of admittance than PDMS coating. The thickness of the polymer coating would affect the amplitude of the sensor's admittance. It has been shown that the thicker the coating, the lower the sensor's amplitude of admittance. The experimental observations and assumptions concur with simulation results.

3. This study also demonstrates the EMI signal of cementitious materials coupled with three types of sensors (uncoated, polyester-coated, and PDMS-coated) from a very early age (6 hours to 12 hours) to an early age (1 day to 7 days). The conductance and susceptance spectrums tend to shift rightward due to the stiffness growth of cementitious materials during the hydration process. The samples with different types of sensors all present a good correlation between EMI-RMSD and mechanical properties (compressive strength and elastic modulus). The regression result (R^2) for all sensors is above 0.95 in monitoring the compressive strength and R^2 is greater than 0.9 in the elastic modulus evaluation of mortar samples. Although polymer coatings slightly affected the sensitivity of the sensor, the polymer-coated sensor still performed excellently at capturing the property changes of cementitious materials.

4. The two types of polymer-coated sensors show the feasibility of monitoring the internal stiffness growth of cementitious materials with high accuracy. Among these two coatings, the polyester coating presents better robustness than PDMS because of the higher interfacial adhesion and surface energy. The properties mentioned above make polyester more favorable as a PZT sensor coating for monitoring mechanical properties of cementitious materials.

Conflict of Interest
There is no conflict of interest.

Supporting Information
The supplementary information is available at https://dx.doi.org/10.30919/es8d1114.

References
[1] D. H. Nguyen, V. T. N. Dao and P. Lura, *Constr. Build. Mater.*, 2017, **134**, 563-573, doi: 10.1016/j.conbuildmat.2016.12.169.

[2] J. W. Bullard, H. M. Jennings, R. A. Livingston, A. Nonat, G. W. Scherer, J. S. Schweitzer, K. L. Scrivener and J. J. Thomas, *Cement Concrete Res.*, 2011, **41**, 1208-1223, doi: 10.1016/j.cemconres.2010.09.011.

[3] C. C. Hung, Y. F. Su and Y. M. Su, *Compos. Part B-Eng.*, 2018, **133**, 15-25, doi: 10.1016/j.compositesb.2017.09.005.

[4] Y. Feng, Y. Su, N. Lu and S. Shah, *Eng. Sci.*, 2019, **8**, 1-10, doi: 10.30919/es8d816.

[5] S. Ghahari, E. Ghafari, P. Hou and N. Lu, *ES Mater. Manuf.*, 2018, **2**, 51-59, doi: 10.30919/esmm5f172.

[6] L. J. Parrott, M. Geiker, W. A. Gutteridge and D. Killoh, *Cement Concrete Res.*, 1990, **20**, 919-926, doi: 10.1016/0008-8846(90)90054-2.

[7] D. Ai, H. Zhu and H. Luo, *Constr. Build. Mater.*, 2016, **111**, 348-357, doi: 10.1016/j.conbuildmat.2016.02.094.

[8] G. Han, Y. F. Su and Luna Lu, *Proc.SPIE*, 2020, **11379**, doi: 10.1117/12.2558261.

[9] Y. F. Su, R. R. Kotian and N. Lu, *Compos. Part B-Eng.*, 2018, **153**, 124-129, doi: 10.1016/j.compositesb.2018.07.018.

[10] G. Han, Y. Su, Y. Feng and N. Lu, *ES Mater. Manuf.*, 2019, **6**, 75-80, doi: 10.30919/esmm5f612.

[11] D. Wang, H. Song and H. Zhu, *Smart Mater. Struct.*, 2014, **23**, 115019, doi: 10.1088/0964-1726/23/11/115019.

[12] Q. Kong, S. Hou, Q. Ji, Y. L. Mo and G. Song, *Smart Mater. Struct.*, 2013, **22**, 085025, doi: 10.1088/0964-1726/22/8/085025.

[13] Y. F. Su, G. Han, A. Amran, T. Nantung and N. Lu, *Constr. Build. Mater.*, 2019, **225**, 340-347, doi: 10.1016/j.conbuildmat.2019.07.164.

[14] E. Ghafari, Y. Yuan, C. Wu, T. Nantung and N. Lu, *Constr. Build. Mater.*, 2018, **171**, 504-510, doi: 10.1016/j.conbuildmat.2018.03.165.

[15] A. Narayanan, A. Kocherla and K. V. L. Subramaniam, *J. Nondestruct. Eval.*, 2017, **36**, 64, doi: 10.1007/s10921-017-0442-4.

[16] Y. F. Su, G. Han, T. Nantung and N. Lu, *Constr. Build. Mater.*, 2020, **259**, 119848, doi: 10.1016/j.conbuildmat.2020.119848.

[17] W. Yan and W. Q. Chen, *Advances in Civil Engineering*, 2010, **2010**, 429148, doi: 10.1155/2010/429148.

[18] Z. Guo and Z. Sun, *Proc. SPIE*, 2012, **8345**, 834524, doi: 10.1117/12.915500.

[19] H. K. Lee and R. Tawie, *Proc. SPIE*, 2009, **7292**, 729223, doi: 10.1117/12.815588.

[20] Y. F. Su, A. Amran, T. Nantung and N. Lu, *The Transportation Research Board (TRB) 98th Annual Meeting*, 2019 of Conference.

[21] X. Lu, Y. Y. Lim and C. K. Soh, *Constr. Build. Mater.*, 2018, **172**, 134-152, doi: 10.1016/j.conbuildmat.2018.03.222.

[22] Y. Yang, B. S. Divsholi and C. K. Soh, *Sensors*, 2010, **10**, 5193-5208, doi: 10.3390/s100505193.

[23] Y. F. Su, G. Han, A. Amran, S. T. Graham and N. L. Lu, *Sensors Smart Struct. Technol. Civ., Mech., Aerosp. Syst.*, *2019*, **10970**, 1097022, doi: 10.1117/12.2513977.

[24] Y. Chen, Y. Wen and P. Li, *Sensor. Actuat. A-Phys.*, 2006, **128**, 116-124, doi: 10.1016/j.sna.2006.01.001.

[25] J. Kim, J. W. Kim and S. Park, *Proc.SPIE*, 2014, **9063**, 906316, doi: 10.1117/12.2044982.

[26] V. G. Annamdas, Y. Yang and C. Soh, *Impedance based Concrete Monitoring using Embedded PZT Sensors*, 2010

[27] D. Wang, J. Zhang and H. Zhu, *Shock Vib.*, 2015, **2015**, 821395, doi: 10.1155/2015/821395.

[28] T. Jothi Saravanan, K. Balamonica, C. Bharathi Priya, N. Gopalakrishnan and S. Murthy, *J. Infrastruct. Syst.*, 2017, **23**, 04017029, doi: 10.1061/(ASCE)IS.1943-555X.0000386.

[29] W. Dong, W. Li, K. Vessalas and K. Wang, *ES Mater. Manuf.*, 2020, **7**, 51-63, doi: 10.30919/esmm5f711.

[30] Z. X. Li, X. M. Yang and Z. Li, *J. Transp. Eng.*, 2006, **132**, 565-573, doi: 10.1061/(ASCE)0733-947X(2006)132:7(565).

[31] V. G. M. Annamdas and C. K. Soh, *Smart Mater. Struct.*, 2006, **15**, 538-549, doi: 10.1088/0964-1726/15/2/037.

[32] Z. Li, L. Qin and S. Huang, *J. Mater. Civil Eng.*, 2009, **21**, 643-647, doi: 10.1061/(asce)0899-1561(2009)21:11(643).

[33] G. Gunduz, D. Erol and N. Akkas, *J. Compos. Mater.*, 2016, **39**, 1577-1589, doi: 10.1177/0021998305051086.

[34] B. E. Schubert and D. Floreano, *RSC Adv.*, 2013, **3**, 24671, doi: 10.1039/c3ra44412k.

[35] F. G. Baptista and J. V. Filho, *IEEE Sens. J.*, 2010, **10**, 1297-1303, doi: 10.1109/jsen.2010.2044037.

[36] X. Lu, Y. Y. Lim and C. K. Soh, *Struct. Health Monit.*, 2018, **17**, 902-918, doi: 10.1177/1475921717725028.

[37] A. Narayanan and K. V. L. Subramaniam, *Constr. Build. Mater.*, 2016, **105**, 536-544, doi: 10.1016/j.conbuildmat.2015.12.148.

[38] P. Negi, T. Chakraborty, N. Kaur and S. Bhalla, *Constr. Build. Mater.*, 2018, **169**, 489-498, doi: 10.1016/j.conbuildmat.2018.03.006.

[39] C. P. Providakis, E. V. Liarakos and E. Kampianakis, *Smart Mater. Res.*, 2013, **2013**, 1-10, 10.1155/2013/932568.

[40] G. Park, H. Sohn, C. R. Farrar and D. J. Inman, *Shock and Vibration Digest*, 2003, **35**, 451-463, doi: 10.1177/05831024030356001.

[41] S. W. Shin, A. R. Qureshi, J. Y. Lee and C. B. Yun, *Smart Mater. Struct.*, 2008, **17**, 055002, doi: 10.1088/0964-1726/17/5/055002.

[42] D. Wang, J. Zhang and H. Zhu, *Shock Vib.*, 2015, **2015**, 821395, doi: 10.1155/2015/821395.

[43] D. Wang and H. Zhu, *Constr. Build. Mater.*, 2011, **25**, 3703-3708, doi: 10.1016/j.conbuildmat.2011.04.020.

[44] D. S. S. Corp, *Abaqus 6.11 Theory Manual*, 2011

[45] A. G. Brooks, A. K. Schindler and R. W. Barnes, *J. Mater. Civil Eng.*, 2007, **19**, 1017-1025, doi: 10.1061/(ASCE)0899-1561(2007)19:12(1017).

[46] G. Trtnik, F. Kavcic and G. Turk, *Ultrasonics*, 2009, **49**, 53-60, doi: 10.1016/j.ultras.2008.05.001.

[47] D. M. F. Madeira, O. Vieira, L. A. Pinheiro and B. de Melo Carvalho, *Int. J. Chem. Eng.*, 2018, **2018**, 2709037, doi: 10.1155/2018/2709037.

[48] J. Comyn, in *General Knowledge, Application Techniques, New Curing Techniques*, ed. P. Cognard, 2006, vol. 2, ch. 1.3.5 Thermodynamic Work of Adhesion.

[49] Solid surface energy data (SFE) for common polymers, http://www.surface-tension.de/solid-surface-energy.htm).

[50] D. Enterprises, Surface Energy Data for PET: Poly(ethylene terephthalate), CAS # 25038-59-9, http://www.accudynetest.com/polymer_surface_data/pet.pdf).

[51] D. Enterprises, Surface Energy Data for PDMS: Polydimethylsiloxane, CAS #9016-00-6, http://www.accudynetest.com/polymer_surface_data/polydimethylsiloxane.pdf).

Publisher's Note

Engineered Science Publisher remains neutral with regard to jurisdictional claims in published maps and institutional affiliations.